Resonant phonon-assisted energy transfer in ruby from 29-cm^{-1}-phonon dynamics

R. S. Meltzer, J. E. Rives, and W. C. Egbert*
Department of Physics, University of Georgia, Athens, Georgia 30602
(Received 11 May 1981; revised manuscript received 1 September 1981)

The dynamics of 29-cm^{-1} phonons resonantly trapped in the $\bar{E} \rightarrow 2\bar{A}$ excited-state resonance of Cr^{3+} ions in Al_2O_3 is studied as a function of excited ion concentration, spot size, and Cr^{3+} concentration employing pulsed optical techniques for generating and detecting the phonons. It is shown that serious differences exist between the present pulsed experiments and the cw optical experiments described elsewhere. The observed saturation of the bottlenecked lifetime at high excited-ion concentrations and its independence of spot size is shown to be consistent with a resonant-phonon-assisted energy transfer (RPAET) among nonresonant ions, which shifts the phonons out of the resonance. Detailed computer calculations of this rate are performed which include a random distribution of Cr^{3+} pairs with an exchange which decays exponentially with separation. Several models are considered for the minimum pair separation which leaves the pairs resonant with the single ions. Calculations for both microscopic and macroscopic broadening are examined. We find that the calculated rates are consistent with the observed magnitude of the saturated lifetime and its dependence on Cr^{3+}-ion concentration assuming microscopic broadening and a value of the exchange an order of magnitude smaller than previously estimated for average pair separations in 1% ruby. Implications for the effects of RPAET on the problem of energy transfer in ruby are discussed and it is shown that the absence of RPAET in fluorescence line narrowing and transient grating experiments is consistent with its dominant role in 29-cm^{-1}-phonon dynamics assuming these smaller values for the exchange.

I. INTRODUCTION

Ruby offers a unique opportunity to study the dynamics of high-energy phonons. The ^2E state of Cr^{3+} in Al_2O_3 is split by 29 cm^{-1} into the $\bar{E}$ (lower) and $2\bar{A}$ (upper) states, as shown in Fig. 1. The resonance is unusually narrow for a resonance between two crystal-field states. At low temperatures relaxation between $2\bar{A}$ and $\bar{E}$ occurs predominantly via a single-phonon process with $T_1 \simeq 1$ ns. 29-cm^{-1} phonons can be generated via the relaxation $2\bar{A} \rightarrow \bar{E}$ which follows optical pumping of the $2\bar{A}$ state directly or optical pumping of the broadbands with the subsequent subnanosecond relaxation of some of the ions to $2\bar{A}$. The resulting 29-cm^{-1} phonons can be detected from the enhanced R_2 luminescence which results from the strong absorption of the resonant phonons by the excited ions in $\bar{E}$. The strong absorption leads to phonon bottlenecking and resonant trapping of the 29-cm^{-1} phonons.

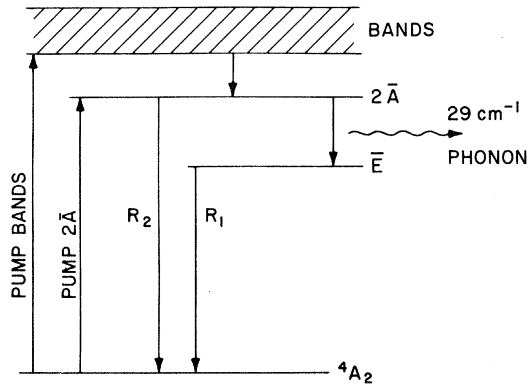

FIG. 1. Energy-level diagram of Cr^{3+} in Al_2O_3 (ruby) showing alternative methods of generating 29-cm^{-1} phonons pumping either the broadbands or $2\bar{A}$ states.

The literature concerned with the dynamics of resonantly trapped 29-cm^{-1} phonons in ruby is quite extensive.[1-17] In the earliest experiments by Renk and Peckenzell[4] in which 29-cm^{-1} phonons from a heat pulse were trapped in an optically excited volume and detected from the enhanced R_2 emission, it was concluded that the phonon lifetime vis-à-vis spontaneous anharmonic breakup was $\simeq 1.5$ μs in 0.075 wt% ruby. Later experiments by Meltzer and Rives[9] using optical techniques to generate only resonant phonons directly within the excited volume suggested values $\simeq 0.5$ μs for anharmonic decay in 0.08 wt% ruby. Later experiments by Pauli and Renk[10] gave closer agreement (0.35 μs) between the two experiments.

Dijkhuis, van der Pol, and de Wijn,[8] using cw exci-

tation into the broadbands of a 0.1% ruby sample to maintain an excited ion density N^* while simultaneously generating resonant phonons in the subsequent $2\bar{A} \rightarrow \bar{E}$ relaxation, concluded from measurements of the R_2/R_1 intensity ratio using 0.3-mm-diam spots at $N^* \simeq 10^{18}$ cm^{-3} that the phonon relaxation time was 10 μs. Further experiments with smaller (120 μm) spots and larger $N^*(\simeq 10^{19}$ cm$^{-3})$ yielded bottleneck factors in excess of 2×10^5, which by applying the same arguments as were used for the 0.3-mm data, give a phonon lifetime of 200 μs, in marked disagreement with the most recent results of the pulsed experiments (1–4 μs).[11–14] Similar work by Kaplyanskii, Basoon, and Shekhtman[15] in very large (1.3-mm diameter) cylindrical volumes yielded bottleneck factors at $N^* \simeq 10^{18}$ cm^{-3}, which are an order of magnitude smaller than observed by Dijkhuis,[8] in their 120-μm-diam spot data for the same N^*. Kaplyanskii concluded that the phonon loss could be explained solely in terms of spatial diffusion and an anharmonic decay time of 2 μs within the theory of Levinson[16] and Malyshev and Shekhtman[17] which treats the resonance as homogeneous with no spectral transfer. Thus not only is there severe disagreement between the pulsed and cw experiments, but considerable inconsistencies appear to exist among the cw experiments themselves.

Using a magnetic field, Dijkhuis and de Wijn[8,13] concluded that for low N^* spatial diffusion governs the phonon loss, but that at larger N^* strong spectral redistribution of the phonons occurs within a Gaussian type resonance of half-width $d\nu_0 \simeq 0.015$ cm^{-1}. They showed that for their largest $N^*(\simeq 10^{19}$ cm$^{-3})$ the phonon distribution broadens to $3d\nu_0$ at zero field. Pauli *et al.*[11] and Pauli and Renk[12] also examined the question of spectral redistribution using cw and combined cw and pulsed techniques and concluded from the observed $N^{*1/2}$ dependence of the lifetime and the behavior of their data on spot size that the resonance is Lorentzian and that the frequency spread of the phonon distribution increases in proportion to $(N^*R)^{1/2}$, reaching a value of 30 $d\nu_0$ for $N^* = 1.5 \times 10^{18}$ cm^{-3}, a value about ten times larger than that obtained by Dijkhuis[8] at that N^*.

Egbert, Meltzer, and Rives[14] have examined the spot size dependence (0.1–0.5 mm) of the temporal response of R_2 emission after pulsed optical excitation of 0.08% ruby. They found that for $N^* > 10^{18}$ cm^{-3}, their data were almost independent of spot size, indicating for the first time the absence of any mechanism requiring spatial transport from the excited volume. In addition, τ saturates at a value of $\simeq 1$ μs in their samples for $N^* > 10^{18}$ cm^{-3}, showing no further increase with N^*. They suggested for an explanation a mechanism first discussed by Holstein, Lyo, and Orbach[18] to explain phonon-assisted electronic energy transfer in ruby whereby the energy mismatch between nearby Cr^{3+} ions is taken up by the 29-cm^{-1} phonon, thereby shifting the phonon's energy out of the narrow $\bar{E} \rightarrow 2\bar{A}$ resonance. The model predicts a saturation of the observed lifetime at high N^*, and using reasonable parameters, a value of $\simeq 1$ μs is obtained from the model, as observed.

Most recently Hu[19] has seen evidence for stimulated emission of transverse 29-cm^{-1} phonons from cylindrically excited regions by pumping directly the R_2 absorption thereby creating a population inversion.

Clearly, our understanding of 29-cm^{-1}-phonon dynamics in ruby is far from complete. The early conclusions which claimed to have measured the anharmonic decay time are probably incorrect. It is reasonably certain that spatial diffusion dominates the loss for small N^* and R, aided by spectral diffusion at moderate N^* and R. For the largest values of N^* other mechanisms which do not involve spatial or spectral diffusion or anharmonic decay must limit the time the resonant phonons remain trapped in the excited volume.

In this paper we present the results and analysis of a comprehensive group of experiments using pulsed optical generation and time-resolved optical detection techniques to measure the 29-cm^{-1}-phonon lifetime as a function of excited-ion resonant-scatterer density, spot size, and ground state Cr^{3+} concentration. The emphasis will be on the moderate and high N^* regime. We show that (1) for large excited ion densities, the behavior of the 29-cm^{-1}-phonon lifetime upon these experimental conditions is consistent with a model in which the phonon lifetime is limited by a resonant-phonon-assisted energy transfer, (2) the observed contribution of RPAET to the phonon loss is compatible with recent experiments in electronic energy transfer in ruby using fluorescence line narrowing,[20] transient grating,[21] and Stark shifting[22] techniques, which indicate very slow nonresonant and resonant energy transfer, providing the values of the exchange contribution to the energy transfer are reduced by at least one order of magnitude compared with previous estimates for average Cr^{3+} separations appropriate to 1% ruby, and (3) serious differences exist between the pulsed and cw experiments and indeed among the cw experiments themselves, which at this point remain totally unresolved.

In Sec. II we discuss the experimental techniques used in the present work. The results of these experiments are examined in Sec. III and compared with those of previous workers. In Sec. IV we present a model to explain the large N^* results using a resonant-phonon-assisted energy transfer, and include a calculation of its magnitude and ruby concentration dependence, which is in reasonable agreement with the experimental results. In Sec. V we discuss the relationship between the phonon and energy-transfer experiments in ruby and finally present our conclusions in Sec. VI.

II. EXPERIMENTAL TECHNIQUES

In this paper we examine the temporal response of the R_2 luminescence as a function of spot-diameter ($0.1\ \text{mm} < 2R < 2\ \text{mm}$) and excited-ion concentration ($1.5\times10^{15}\ \text{cm}^{-3} < N^* < 1.5\times10^{19}\ \text{cm}^{-3}$) for three different Cr^{3+} ground-state concentrations. In all experiments the samples were fully immersed in liquid helium at 1.5 K.

The samples were typically 3 to 5 mm on a side and had concentrations of 0.023, 0.081, and 0.28 wt% Cr_2O_3/Al_2O_3, as determined spectroscopically.[23] The spot size was controlled using masks directly in front of the samples with pinholes varying from 0.1 to 2.5 mm in diameter. The laser spot size was usually a factor of 2 larger than the pinholes to minimize nonuniform excitation across the illuminated regions. N^* was estimated in the pulsed-excitation experiments from the known absorption coefficients and laser-pulse energies and where cw excitation was employed, the absorption coefficient at 5140 Å along with the ^2E radiative lifetime, including effects of radiation trapping, were utilized.

In order to cover the large range of R and N^*, and in an attempt to minimize sample heating which occurred with the largest excitation energies, experiments were carried out using a variety of excitation techniques. In this section we describe six types of experiments employed.

1. cw pumping with a xenon lamp and a N_2-pumped dye laser. Some of the data included in this paper were presented previously[9] when a high-pressure xenon lamp was utilized to prepare a metasable ^2E population in conjunction with a N_2-pumped dye laser pumping the broadbands to prepare the 29-cm^{-1} resonant phonons in the subsequent relaxation from $2\bar{A}$ and $\bar{E}$. These experiments covered the low-N^* range for large spot sizes ($2R = 1$ mm). The R_2 emission was viewed parallel to the xenon lamp and laser excitation. Filters were used to remove the R_2 wavelength from the xenon-lamp excitation. Thin samples (~ 1 mm) were used to minimize N^* variation through the excitation cylinder.

2. Broadband excitation with a N_2 laser-pumped dye laser. For small spot size ($2R < 200\ \mu\text{m}$) it was possible to cover nearly the full range of N^* using a N_2 laser-pumped dye laser pumping into the broadband absorption with up to 250 μJ in a 3-ns pulse. The R_2 luminescence was collected over a small section of the excitation cylinder (to minimize N^* variation across the absorption path) by looking perpendicularly to the cylinder axis. Time-resolved spectra in this and the previous technique were obtained using a single-photon time-correlation technique described previously.[24]

3. Broadband excitation with a coaxial flashlamp pumped tunable dye laser. In order to obtain high values of N^* in larger excitation volumes, a flashlamp-pumped tunable dye laser was employed. With a Littrow grating in the cavity, up to 70 mJ of light at 5800 Å were obtained in a 700-ns pulse. Because the laser pulse length is comparable to the phonon decay time, we inserted a Pockels cell in the laser cavity, which acted as a Q switch, to abruptly terminate laser action with a fall time of about 20 ns. This allowed us to examine the R_2 decay immediately after the peak power point of the laser without the complication of simultaneous phonon and N^* generation. This attempt was only moderately successful because when more than 5 mJ were injected into the sample, sufficient heating of the sample occurred such as to make it impossible to examine the resonant phonon dynamics. A major part of the heating results from the nonradiative multiphonon relaxation between the broadband states and the ^2E states converting approximately 20% of the absorbed light energy into high-energy phonons. Further relaxation within the sample results in a thermal distribution of phonons over the full sample volume corresponding to a temperature well above that of the bath. It is this crystal heating which is seen by our optical detector of 29-cm^{-1} phonons at times well in excess of the bottlenecked relaxation times τ.

With the flashlamp-pumped laser, the R_2 luminescence was sufficiently strong to give an analog signal rather than individual pulses on our fast photomultiplier (Amperex TVP56). We stored the signal from a single flash on a 500-MHz transient recorder (Biomation 6500) and between flashes transferred the data digitally to a signal averager.

4. Resonant excitation to $2\bar{A}$ with a coaxial flashlamp laser using external injection. In order to avoid the multiphonon relaxation, we pumped directly to the $2\bar{A}$ level with the flashlamp-pumped tunable dye laser. In order to narrow the bandwidth sufficiently to couple to the 0.2-cm^{-1} absorption bandwidth we injected a 0.2-cm^{-1} 10-ns pulse from a N_2-pumped tunable dye laser. The flashlamp laser cavity was Q spoiled with a Pockels cell until injection. The cavity was left in a high-Q condition until broadband laser radiation began to build up at which point laser action was terminated with the Pockels cell. Using 10^{-4}-M Oxazine 720 in methanol we were able to obtain up to 35 mJ with a 0.2-cm^{-1} bandwidth in a 300-ns pulse. Although the crystal heating was reduced, it remained a problem at the highest pulse energies.

5. Argon-ion laser excitation followed by pulsed excitation into the broadbands. To further avoid crystal heating, experiments were carried out with an argon-ion laser pumping the broadbands at 5140 Å, maintaining a large value of N^* in the $\bar{E}$ state. A pulsed N_2-pumped dye laser exciting the broadbands was used to generate the 29-cm^{-1} phonons but with sufficiently low energy that N^* was not substantially affected. The relative number of ions excited by the two lasers could be determined by watching the in-

crease in the R_1 luminescence due to the pulsed laser after the 29-cm^{-1}-phonon decay ceased. The observed relative increase agreed with our relative estimated values of N^* due to the individual lasers. When cw power in excess of 1 W was focused on the sample, bubbling of the helium (normally 1.7 K) prevented the use of the maximum argon-ion laser power. For the larger spot sizes, the pulsed N_2-pumped dye laser was replaced by the flashlamp-pumped dye laser, however at relatively low pulse energies (<1 mJ) to improve the signal to noise ratio in these large volumes.

6. Flashlamp- and N_2-pumped dye laser broadband excitation. For maximum values of N^* in the larger spot sizes, use was made of both pulsed laser systems tuned to the broadband absorption at ~ 5800 Å. The flashlamp-pulsed dye laser prepared a large value of N^*. The N_2-pumped dye laser which generated a small pulse of 29-cm^{-1} phonons was delayed up to 200 μs to allow the crystal to return to thermal equilibrium before the nonequilibrium resonant phonon population was generated.

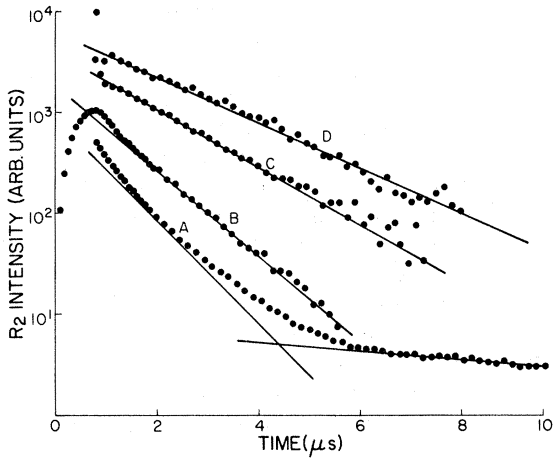

FIG. 2. Typical experimental results of the temporal response of the R_2 emission under varying experimental conditions. A: Single 0.15-mJ 3-ns pulse at 5800 Å in a 250-μm-diam spot. B: Single 0.5-mJ 700-ns pulse at 5800 Å in a 200 μm diam spot. C: 150-mW cw argon laser plus 50-μJ 3-ns pulse pumping $2\bar{A}$ in an 800-μm-diam spot. D: 15-mJ 700-ns pulse at 5800 Å followed by a delayed 200-μJ 3-ns pulse at 5800 Å.

III. RESULTS

In this section we summarize the results of all the experiments described in Sec. II in order to obtain an overall picture of the 29-cm^{-1}-phonon dynamics over a broad range of N^*, R, and Cr^{3+} concentration. Before presenting these results we discuss typical experimental data from a few of these experiments showing especially some of the difficulties encountered in interpreting the results.

In those experiments in which a single laser was used to both prepare N^* and to generate the phonons, the R_2 decay was not purely exponential as illustrated in Fig. 2 (curve A). In this example, a 0.15-mJ 3-ns pulse at 5800 Å excited the 0.081% sample in a 250-μm-diam spot. The background level (shown for curve A) which is generally present, was first subtracted from the raw data. The background exhibits a decay and may result from a return to thermal equilibrium after heating of the sample by the excitation pulse. A local heating of the excited volume to 5 K due to the large fraction of light energy which is converted to high-energy phonons in the multiphonon relaxation from the broadbands (0.03 mJ) is all that would be required. The data corrected for the background show an exponential decay over two decades except during the first ~ 1 μs. This enhanced decay at early times is very typical of that seen in experiments where a single pulsed laser is used to both produce a large value of N^* and generate the phonons. Some enhanced decay at early times is expected since initially only 72% of the excited ions are in the lower state after relaxation from the broadband states. The effect, however, is much too great to be explained in this way. It appears that the phonons escape more rapidly initially. Although stimulated emission of 29-cm^{-1} phonons in ruby has been observed,[19] a population inversion is not produced in pumping the broadbands. It could play a role in those experiments in which R_2 was directly excited although we have seen no evidence for it.

The initially enhanced decay is also observed in experiments in which the broadbands were pumped with a long (700-ns) pulse as shown in curve B of Fig. 2. Here a 200-μm-diam spot was excited with 0.5 mJ. Note the more rapid decay during the first 0.5 μs after the excitation has ceased. Aside from this deviation, the decay follows a pure exponential for over two decades.

When, however, N^* is prepared with an argon laser or a preceding flashlamp laser pulse and the resonant phonons are prepared with a weak pulse from a N_2-pumped dye laser, this initially enhanced decay is not observed as shown in Fig. 2, curves C and D, respectively. In curve C, obtained with 150 mW of cw power focused to a 800-μm spot, the sharp spike at $t=0$ results from scattered R_2 laser light off the sample from the 50-μJ dye laser pulse in resonance with the spectrometer. For curve D, a 15-mJ flashlamp-pumped dye laser pulse focused on a 1-mm-diam spot prepared N^*. A 200-μJ pulse from the N_2-pumped dye laser, also tuned to the broadband absorption but delayed about 200 μs to allow the sample to cool from the first pulse, was used to generate the 29-cm^{-1} phonons.

Attempts to use the flashlamp-pumped dye laser

alone were restricted to pulse energies < 5 mJ. This is illustrated in Fig. 3. Curve A, in which 3.5 mJ was focused onto a 500-μm spot, shows a slight nonexponential behavior at long times which is a precursor of sample heating. When 7 mJ are focused on the same spot, a noticeable hump and tail are observed extending to about 20 μs (curve B). When 18 mJ are focused on the sample, (1.8-mm spot) a pronounced heating occurs (curve C). The heating persists for almost 1 ms (see insert). We compared the time dependence of the intensity of the R_2 and R_1 emission, and found, after correction for the difference in their transition probabilities, that initially the $2\bar{A}$ to $\bar{E}$ population ratio is about 0.4 as predicted from the known branching ratio in the relaxation from the broadbands.[25] This corresponds to an effective initial resonant-phonon temperature of ~ 50 K. However, even after the resonant phonons have escaped the excited volume, the R_2/R_1 intensity ratio indicates a bulk sample temperature of ~ 30 K, which results from the thermalized burst of high-energy phonons accompanying the multiphonon relaxation from the broadbands.

We now discuss the phonon dynamics in 0.081% ruby as a function of N^* and $2R$. These results are a composite obtained from all of the experiments described in Sec. II which do not exhibit heating effects and appear in Fig. 4. The lines drawn through the data serve only as guides to the eye. The relative uncertainties in N^* are probably $< \pm 10\%$ in any given series of experiments using a single technique. However the relative uncertainties in comparing data

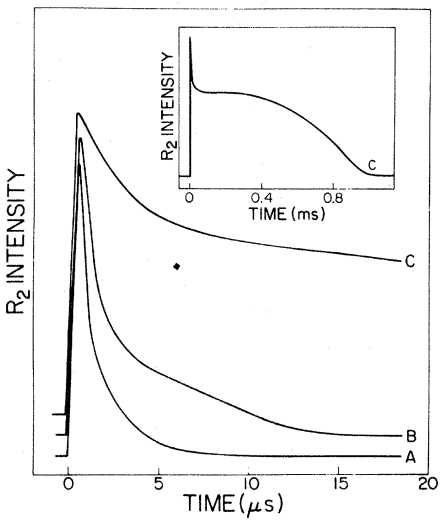

FIG. 3. Temporal response of the R_2 emission showing heating effects for large laser pulse energies: A: 3.5-mJ 700-ns pulse at 5800 Å in a 500-μm-diam spot. B: 7-mJ 700-ns pulse at 5800 Å in a 500-μm diam spot. C: 18-mJ 700-ns pulse at 5800 Å in a 1.8-mm-diam spot.

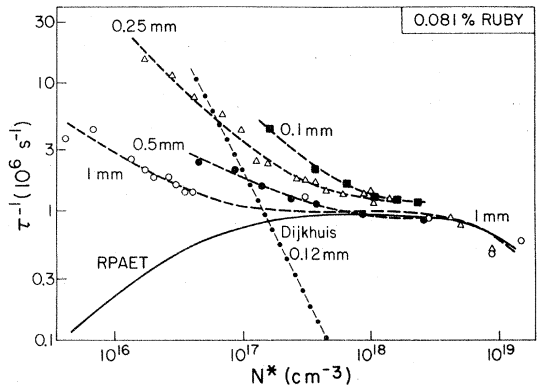

FIG. 4. Decay rate of the R_2 emission in 0.081% ruby as a function of excited ion density for several spot sizes. The dashed curves are guides to the eye. The dash-dot curves are calculations based on the cw excitation data of Dijkhuis and de Wijn (Ref. 13) and are shown for comparison purposes. The solid curve is based on a model calculation discussed in Sec. V.

taken using different techniques are probably no better than $\pm 30\%$. The absolute scale on N^* is also estimated as $\pm 30\%$.

The most prominent feature of these data is the change in the spot-size dependence of the relaxation rate as a function of N^*. At low N^* ($\simeq 10^{16}$ cm^{-3}), τ^{-1} is strongly dependent on $2R$ [$\tau^{-1} \propto (2R)^{-x}$; $x > 1$], whereas for $N^* > 10^{18}$ cm^{-3}, τ^{-1} is independent of $2R$. It is also evident that for low N^*, $\tau^{-1} \propto N^{*-y}$, $0.5 < y < 1$ while for $N^* > 5 \times 10^{17}$ cm^{-3}, τ^{-1} is nearly independent of N^*, especially for the larger spot sizes. While various theories for spatial and spectral diffusion predict different dependencies of τ^{-1} on spot size and N^*, none of them predict an independence of these quantities. This independence implies a mechanism which does not involve spatial diffusion from the excited volume. Although the low-N^* data are insufficient to obtain the exact relationship between τ^{-1} and N^* or $2R$, the independence at large N^* is quite clear. One further important point is the additional decrease in τ^{-1} at the highest N^*. We shall return to this later, simply noting for the present that at these values of N^*, the ground-state population is being significantly depleted ($n_0 = 2.5 \times 10^{19}$ cm^{-3}).

In Fig. 5 we show the phonon dynamics for 0.023% ruby as a function of N^* and $2R$. Qualitatively the behavior is similar to that of 0.081% ruby. At low N^*($\simeq 10^{16}$ cm^{-3}) there is a strong spot-size dependence of τ^{-1} with $\tau^{-1} \propto R^{-2}$ as would be expected for pure spatial diffusion while at large $N^* \simeq 10^{18}$ cm^{-3}, τ^{-1} is nearly independent of spot size. Unlike the 0.081% data, only the large spot-size data exhibit a τ^{-1} independent of N^*. Note, however, that in the 0.081% results the smaller spot sizes show an N^* independence only over a more restricted range of N^*.

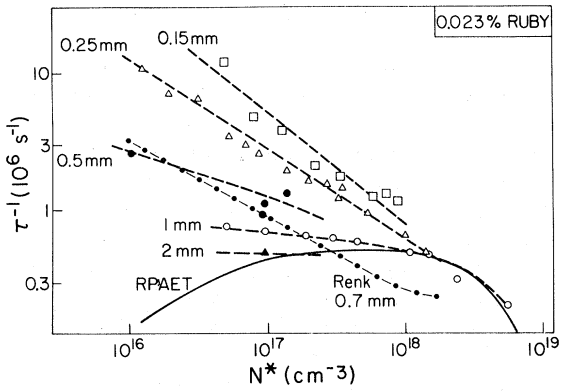

FIG. 5. Decay rate of the R_2 emission in 0.023% ruby as a function of excited-ion density for several spot sizes. The dashed curves are guides to the eye. The dash-dot curve is a smoothed representation of the data of Pauli *et al.* (Ref. 11) in 0.03% ruby. The solid curve is based on a model calculation discussed in Sec. V.

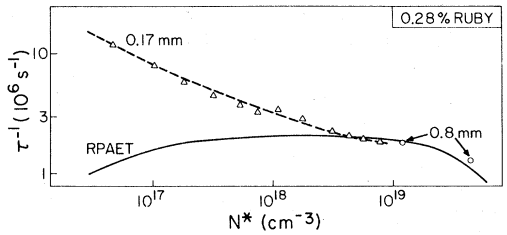

FIG. 6. Decay rate of the R_2 emission in 0.28% ruby as a function of excited-ion density. The dashed curve is a guide to the eye. The solid curve is based on a model calculation discussed in Sec. V.

In general the 29-cm^{-1}-phonon relaxation rates are lower in 0.023% ruby than 0.081% at a particular $2R$ and N^*. However, at low N^*, $\tau^{-1} \propto N^{*-y}$, $0.5 < y < 1$, as was the case for 0.081% ruby. This result is consistent with previous conclusions of Pauli *et al.*[11] who found for $2R = 700$ μm in 0.03% ruby $\tau^{-1} \propto N^{*-1/2}$ (dash-dot curve in Fig. 5). However, Pauli observed $\tau^{-1} \simeq 2.5 \times 10^5$ s^{-1} for $N^* = 1.5 \times 10^{18}$ cm^{-3} which is a factor of 2 smaller than the value observed for 0.023% ruby in the present experiments. We do, however, observe this rate by $N^* \simeq 5 \times 10^{18}$ cm^{-3}. It is possible that our relative N^* scales could differ by a factor of 2 or 3. A further similarity to the 0.081% data is the noticeable decrease in τ^{-1} at the largest value of N^* when the ground-state population ($n_0 = 7 \times 10^{18}$ cm^{-3}) is significantly depleted.

When we compare the present results with those of Dijkhuis and de Wijn[13] using cw techniques the disagreement is striking. Dijkhuis and de Wijn's results using the relation $\tau^{-1} = T_1^{-1}/b$ (dash-dot curve in Fig. 4) for $2R = 120$ μm in 0.1% ruby show $\tau^{-1} \simeq N^{*-2}$ up to $N^* \simeq 10^{18}$ cm^{-3} with no tendency toward saturation at large N^*. It appears as if quantitative agreement between the two results is being approached at $N^* \simeq 5 \times 10^{16}$ cm^{-3}, but at larger N^* the behavior of τ^{-1} with N^* is not even qualitatively in agreement. By $N^* = 3.4 \times 10^{18}$ cm^{-3} (not shown in Fig. 4) Dijkhuis finds $\tau^{-1} \simeq 4.5 \times 10^3$ s^{-1}, almost 3 orders of magnitude smaller than the values obtained by oursleves and Renk using pulsed techniques.

In 0.28% ruby (Fig. 6) we find $\tau^{-1} \propto N^{*0.4}$ over a wide range of $N^*(4 \times 10^{16}$ $cm^{-3} < N^* < 2 \times 10^{18}$ $cm^{-3})$ with a saturation occurring above $N^* \simeq 10^{19}$ cm^{-3}. We did not do an extensive spot-size study but at $N^* \simeq 10^{19}$ cm^{-3} it appears that τ^{-1} is identical for $2R = 0.17$ mm and 0.8 mm. We note that the saturation value of $\tau^{-1} \simeq 1.7 \times 10^6$ s^{-1} is almost a factor of 2 greater than that observed in 0.081% ruby and almost a factor of 4 greater than that observed in our 0.023% sample. We will discuss this in the next Sec. IV.

IV. PHONON LOSS BY RESONANT PHONON-ASSISTED ENERGY TRANSFER

Electronic energy transfer between nonresonant Cr^{3+} ions in ruby has been extensively studied experimentally by a number of groups.[20,21] Holstein, Lyo, and Orbach[18] considered several phonon-assisted processes which could lead to the observed transfer rates and concluded that the dominant process is a resonant two-phonon-assisted energy transfer (RPAET) pictured in Fig. 7. The energy mismatch δ between the two Cr^{3+} ions is due to crystal-field inhomogenieties. The circled numbers indicate the order of transitions. For the one-site process shown in Fig. 7(a) a Cr^{3+} ion at site 1 initially excited to the $\bar{E}$ state first absorbs a 29-cm^{-1} phonon taking it to the $2\bar{A}$ state. This is followed by the emission of a $29 + \delta$-cm^{-1} phonon and finally by transfer of the ex-

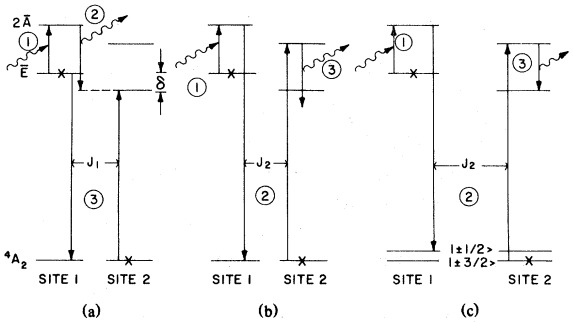

FIG. 7. Schematic diagram of phonon-energy shifting by resonant two-phonon-assisted energy transfer (RPAET) in ruby. (a) One-site transfer process on site 1; (b) two-site transfer process; (c) phonon-energy shifting due to the ground-state splitting.

citation energy to the ion at site 2 via the exchange coupling J_1 between the ground state and the $\bar{E}$ state. Since the phonon energy shift δ (typically 0.1–0.5 cm^{-1} in ruby) is much larger than the $2\bar{A} \rightarrow \bar{E}$ resonance width of $\simeq 0.015$ cm^{-1} the emitted phonon is nonresonant and will escape the excited volume of the crystal ballistically. The similar transfer mechanism with the phonon processes taking place at site 2 is not shown in Fig. 7, but must be included in the calculations. The two-site process shown in Fig. 7(b) initiates with resonant absorption of a 29-cm^{-1} phonon at site 1 followed by transfer of energy to site 2 with the emission of $29+\delta$-cm^{-1} phonon at site 2. In this case J_2 represents the exchange coupling between the ground state and the $2\bar{A}$ state. Corresponding to the processes depicted in Figs. 7(a) and 7(b) are contributions which occur when the ion initiates and terminates on different ground-state levels which produce an additional energy shift of 0.38 cm^{-1} as shown in Fig. 7(c).

These processes produce an energy-transfer rate[18] between a pair of Cr^{3+} ions

$$W_{\rm Cr}^{\rm res}(J,\delta)=\left[J_1^2+\frac{\delta^2 J_2^2}{\delta^2+\Gamma(2\bar{A})^2}\right]\times\frac{[1+\exp(\delta/kT)]}{\delta^2}W_{\bar{E}\rightarrow 2\bar{A}}\ , \quad (1)$$

where $\Gamma(2\bar{A})$ is the $\bar{E}\rightarrow 2\bar{A}$ phonon absorption homogeneous linewidth and $W_{\bar{E}\rightarrow 2\bar{A}}=T_1^{-1}\times\exp(-\Delta/kT)$ is the phonon absorption rate with $T_1=10^{-9}$ s[21] and $\Delta=29$ cm^{-1}. For the case at hand, $\Gamma(2\bar{A})\ll\delta\ll kT$ and Eq. (1) reduces to

$$W_{\rm Cr}^{\rm res}(J,\delta)=\frac{4J^2}{\delta^2}W_{\bar{E}\rightarrow 2\bar{A}}\ , \quad (2)$$

where we have set $J^2=(J_{\bar{E}}^2+J_{2\bar{A}}^2)/2$. Hereafter we shall denote J_1 and J_2 by $J_{\bar{E}}$ and $J_{2\bar{A}}$, respectively.

If we assume that each Cr^{3+} ion energy transfer is accompanied by the loss of a resonant phonon by energy shifting, then by detailed balance the phonon loss rate due to that pair, $W_{\rm ph}^{\rm res}(J,\delta)$ is given by

$$W_{\rm ph}^{\rm res}(J,\delta)N_{\rm ph}=W_{\rm Cr}^{\rm res}(J,\delta)N^*P(J,\delta)\ , \quad (3)$$

where N^* is the density of excited Cr^{3+} ions, $P(J,\delta)$ is the probability of finding a pair with J and δ, $N_{\rm ph}=\Sigma\bar{p}$ is the density of 29-cm^{-1} phonons, where Σ is the number of phonon modes within the excited state resonance width and $\bar{p}=(e^{\Delta/kT}-1)^{-1}$ is the average population of each mode. Thus

$$W_{\rm ph}^{\rm res}(J,\delta)=\frac{4J^2}{\delta^2}\frac{N^*}{\Sigma}T_1^{-1}P(J,\delta)\frac{\exp(\Delta/kT-1)}{\exp(\Delta/kT)}\ , \quad (4)$$

which becomes

$$W_{\rm ph}^{\rm res}(J,\delta)\simeq\frac{4J^2}{\delta^2}\frac{N^*}{\Sigma}T_1^{-1}P(J,\delta) \quad (5)$$

when $\bar{p}$ (or the effective phonon temperature) is small.

Although immediately after the laser excitation pulse the spin temperature as well as the resonant phonon temperature (and $\bar{p}$) are both quite large ($T_s\simeq T_{\rm ph}\gg\Delta/k$), the exponential decay times are evaluated at later times when $\bar{p}\ll 1$ and $T_{\rm ph}\ll\Delta/k$, thus making Eq. (5) valid in the experimental analysis.

An expression identical to Eq. 5 was recently obtained by Holstein, Lyo, and Orbach[26] by direct calculation of the phonon frequency shifting due to RPAET.

For pairs in which ions are strongly coupled ($J/\delta\gtrsim 1$), the eigenstates of the pair become symmetric (+) or antisymmetric (−) linear combinations of basis states with ion 1 excited and ion 2 excited, whose eigenvalues are

$$E_{\substack{+\\(-)}}=\left(\begin{matrix}+\\-\end{matrix}\right)\tfrac{1}{2}(4J^2+\delta^2)^{1/2}\equiv\left(\begin{matrix}+\\-\end{matrix}\right)\epsilon_0\ . \quad (6)$$

In this circumstance, the resonant-phonon scattering can best be viewed as resonant-phonon absorption from one component of the $\bar{E}$ pair states to a component of the $2\bar{A}$ pair states, followed by emission of a phonon to the initially unoccupied $\bar{E}$ pair state as shown in Fig. 8. We should therefore make the replacement $\delta^2\rightarrow(4J^2+\delta^2)$ in Eq. (5) since this represents the true phonon energy shift.

The total phonon loss rate due to RPAET must include a sum over all Cr^{3+} pairs taking into account the spatial dependence of the site-site coupling $J(r)$ and the distribution of energy mismatch δ. We carry out the sum as a double integration over δ and r. In

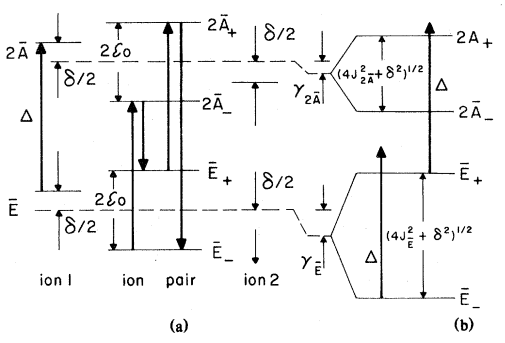

FIG. 8. Energy levels of Cr^{3+} pairs in the presence of pair interactions. (a) Energy levels in the presence of identical exchange in the $\bar{E}$ and $2\bar{A}$ states, where $\epsilon_0=\frac{1}{2}(4J^2+\delta^2)^{1/2}$. Note that Δ, the energy of phonons produced at noninteracting single-ion sites, is still in resonance with the ion-pair states. (b) Energy levels in the presence of different exchange $J_{\bar{E}}$ and $J_{2\bar{A}}$ as well as different energy shifts of the single-ion states, $\gamma_{\bar{E}}$ and $\gamma_{2\bar{A}}$. Note that Δ is no longer in resonance with the ion-pair states.

all calculations of the present work, J and δ are totally uncorrelated. Since J is a function only of r, the pair probability function $P(J,\delta)$ can be separated

$$P(J,\delta)=\rho(r)P(\delta) \ , \tag{7}$$

where $\rho(r)$ is the radial density of Cr^{3+} ions, which in a purely random model is just $4\pi r^2 n_0$, and n_0 is the ground-state Cr^{3+} concentration. $P(\delta)$ is the probability distribution of energy mismatch δ given by

$$P(\delta)=\int_0^\infty g(E)[g(E+\delta)+g(E-\delta)]dE \ , \tag{8}$$

where $g(E)$ is the probability of finding an ion of excitation energy E. The nature of the inhomogeneous broadening has been the subject of much debate. At present it is still not clear whether the inhomogenieties are microscopic or macroscopic in nature. For the purpose of these calculations we treat separately the case of pure microscopic broadening and total absence of microscopic broadening (no local energy mismatch). For the case of microscopic broadening with a Gaussian distribution of energies

$$g(E)=(2\pi\Delta E^2)^{-1/2}\exp[-(E-E_0)^2/2\Delta E^2] \ . \tag{9}$$

E_0 is the energy at the peak of the $\bar{E}$ optical absorption and ΔE is related to δE, the full width at half maximum (FWHM) of the optical absorption line, by the expression $(\Delta E)^2=0.18(\delta E)^2$. For macroscopic broadening $\delta=0$ and $P(\delta)=1$.

For the case where there is no energy shift due to the ground-state splitting this gives

$$W_{\rm ph}^{\rm res}({\rm tot})=4bT_1^{-1}\int_{R_0}^\infty\int_{\delta_{\rm min}}^\infty P(\delta)\rho(r)\frac{J^2(r)}{4J^2(r)+\delta^2}d\delta dr \ , \tag{10}$$

where $4J^2+\delta^2$ is the true energy mismatch including the effects of the coupling as discussed above. Energy shifts less than the $\bar{E}\rightarrow 2\bar{A}$ resonance width will not shift the phonon frequency out of resonance and hence are excluded by choosing $\delta_{\rm min}$ such that $(4J^2+\delta^2)^{1/2}\geq h\Delta\nu_{\rm res}$, where $\Delta\nu_{\rm res}$ is the $\bar{E}\rightarrow 2\bar{A}$ resonance width. For the cases where the ground-state splitting is included in the energy mismatch, the term in the denominator, $4J^2+\delta^2$ must be replaced by the term

$$[(4J^2+\delta^2)^{1/2}\pm 0.38]^2 \ .$$

In order to compare the predicted phonon loss rate from Eq. (10) with the experimentally observed rates, τ^{-1}, it is necessary to consider the phonon dynamics and the Cr^{3+} system in more detail. In the absence of energy transfer the 29-cm^{-1} phonons are resonantly absorbed and reemitted by the excited Cr^{3+} ions. If $\tau_{\rm res}$ is the average propogation time for a phonon then $\tau_{\rm res}/(\tau_{\rm res}+T_1)$ is the relative time the 29-cm^{-1} energy spends as a phonon. The ratio $T_1/\tau_{\rm res}$ can also be expressed as the ratio of available spin states to the number of resonant-phonon states, $N^*/\Sigma\equiv b$. Thus the fraction of time the energy exists as a phonon is just

$$\frac{\tau_{\rm res}}{(T_1+\tau_{\rm res})}=\frac{1}{1+b} \ . \tag{11}$$

Hence the observed rate is

$$\tau^{-1}=W_{\rm ph}^{\rm res}({\rm tot})/(1+b) \ . \tag{12}$$

For dilute ruby $\Sigma=3.5\times10^{16}$ cm^{-3}, so for $N^*\geq 10^{18}$ cm^{-3} ($b>>1$) the RPAET process predicts a phonon loss rate which is independent of N^* in agreement with the present observations. The mechanism is independent of spot size for all N^*, again consistent with experiment at large N^*.

For the radial dependence of the site-site exchange coupling we follow the superexchange model of Lyo[27] with an exchange of the form

$$J(r)=J_0\exp(-ar) \ . \tag{13}$$

For parameters appropriate to ruby, Lyo finds $a\simeq 1$ $Å^{-1}$.

The selection of a value for R_0, the lower limit of integration in Eq. (7) is quite subtle and represents a severe limitation on our ability to calculate an absolute value for τ^{-1}. Clearly the excited levels corresponding to the single-ion ^2E states of the nearest pairs (1st–4th nearest neighbors) cannot interact resonantly with the 29-cm^{-1} phonons produced at single-ion sites since the well-known energy-level structures of the pair states do not exhibit any 29-cm^{-1} resonances. At what value of R_0 does the resonance condition reappear? Off resonance can occur for many reasons when the energy shifts or splittings of the $\bar{E}$ and $2\bar{A}$ states due to the presence of the nearby Cr^{3+} ion are not identical as indicated in Fig. 8(b). The factors which can contribute to this lack of resonance include (1) different exchange splittings and energy-transfer matrix elements for the $\bar{E}$ and $2\bar{A}$ states expected due to the different phase factors entering the sum of two electron exchange integrals for these two single-ion states,[28] (2) variations in the single-ion trigonal field of each Cr^{3+} ion of the pair due to the presence of the other nearby Cr^{3+} ions which alters the $\bar{E}\rightarrow 2\bar{A}$ splitting energy, and (3) differences in the Racah parameters for the $\bar{E}$ and $2\bar{A}$ states of the strongly coupled ions of the pair relative to those of the single ions leading to different shifts of the $\bar{E}$ and $2\bar{A}$ states. Mechanisms (2) and (3) give rise to the different shifts $\gamma_{\bar{E}}$ and $\gamma_{2\bar{A}}$ also shown in Fig. 8(b).

A proper treatment of all of these effects from first principles would be impossible at the present time, and even if it were possible, it would have to be car-

ried out separately for all of the many strongly coupled ($J/\delta \gtrsim 1$) pairs. We have therefore chosen to approach the calculation of τ^{-1} from two extreme points of view. In the first, referred to as Model 1, we consider only mechanism (1), the exchange itself, as the cause for resonance failure. It is assumed that because of the difference in the phase factors for the $\bar{E}$ and $2\bar{A}$ states, which enter into the sum of two electron exchange integrals in determining the total exchange interaction,[28] there is no correlation between the exchange of the $\bar{E}$ and $2\bar{A}$ states. We therefore take the exchange in the $\bar{E}$ state $J_{\bar{E}}$ equal to twice the exchange in the $2\bar{A}$ state, $J_{2\bar{A}}$, so that the difference between the exchange interaction $J_{\bar{E}} - J_{2\bar{A}}$ is of the order of either $J_{\bar{E}}$ or $J_{2\bar{A}}$ or their average J. In this model, R_0 is determined by the Cr^{3+} ion separation for which

$$\tfrac{1}{2}(4J_{\bar{E}}^2+\delta^2)^{1/2} - \tfrac{1}{2}(4J_{2\bar{A}}^2+\delta^2)^{1/2} = h\Delta\nu_{\text{res}} \ .$$

It is a function of the single-ion energy mismatch of the ions in the pair. To the extent that this overestimates their difference, we underestimate the contribution of RPAET. To the extent that we ignored mechanisms (2) and (3) we overestimate the contribution of RPAET.

In the second point of view, Model 2, we ignore mechanism (1) and assume that the off-resonance condition is produced solely by mechanisms (2) and (3) which result from the presence of the other member of the Cr^{3+} pair at a nearby site. We assume that the difference between the $\bar{E} \rightarrow 2\bar{A}$ transition energy of the pair and that of the single ions varies monotonically with distance, which results in a cutoff R_0 which is independent of Cr^{3+} concentration, depending only on the Cr^{3+} separation of the pair. As a consequence, the increased optical linewidth δE, which accompanies an increase in concentration, results in a reduced contribution to RPAET of any single pair of ions separated by distance r because of the proportional increase in their energy mismatch δ which follows from a microscopic model for the broadening as discussed above.

We first consider the results of Model 1 with microscopic broadening. The integrals in Eqs. (8) and (10) were computed numerically for several values of the parameter a. For each choice of a, J_0 was determined from the best fit to the 0.081% data. The results for $a = 1.0$ Å^{-1}, $J_0 = 1.1$ cm^{-1} are compared with the experimental results at these concentrations in Table I. The calculated asymptotic value of τ^{-1} would be linear in n_0 as seen from Eq. (7), were it not for the variation in optical linewidth δE which was included in the calculation as estimated from optical linewidth studies of ruby. The inclusion of the concentration dependence of δE reduces the concentration dependence of τ^{-1} from a factor of 12 (the range of concentrations) to 6, which brings it more in line with the observed variation of a factor of 3.4. In the calculation it was assumed that the inhomogeneous part of the phonon-resonance width increased in proportion to δE with concentration as shown in Table I.

TABLE I. Comparison of calculated and experimental phonon loss rates at large N^* for Model 1 with microscopic broadening.

Cr^{3+} conc. (wt%)	δE (cm^{-1})	$h\Delta\nu_{\text{res}}$ (cm^{-1})	$\tau^{-1}(10^6$ s$^{-1})$ Calc. RPAET	Expt.
0.023	0.15	0.016	0.39	0.5
0.081	0.2	0.019	1.0[a]	1.0
0.28	0.3	0.026	2.44	1.7

[a] J_0 was varied to produce fit to 0.081% data. Result with $a = 1$ Å^{-1}, $J_0 = 1.1$ cm^{-1}.

The values of J_0 which fit the 0.081% data for this and other values of a are shown in Table II along with values of J for 3.5-Å and 13-Å pair separations. These are values appropriate to 4th nearest-neighbor pairs and average pair separations in 1% ruby, respectively. These values of the exchange are significantly smaller than other estimates. The exchange interaction of 4th nearest-neighbor pairs ($r = 3.5$ Å) can be estimated from the work of Allen, Macfarlane, and White[28] on the exciton spectrum of Cr_2O_3. They obtained a value of ~ 10 cm^{-1} for a single pair. Birgeneau[29] has made an estimate of the exchange at 13 Å from Imbusch's[30] measurements of nonresonant energy transfer between single ions and pairs in 1% ruby and finds $J = 2.5 \times 10^{-3}$ cm^{-1}. Many assumptions were involved in this estimate including a nonstochastic treatment of the ion separation, a long-wavelength approximation for the ~ 100-Å phonons, and estimates of the strain differences for both the

TABLE II. Values of J_0 for Model 1 which fit the observed RPAET rate τ^{-1} for several values of a and the corresponding magnitude of the exchange at $r = 3.5$ Å and $r = 13$ Å.

a (Å^{-1})	J_0 (cm^{-1})	J(3.5 Å) (cm^{-1})	J(13 Å) (10^{-3} cm^{-1})
1.0	1.1	0.033	0.0025
1.2	3.3	0.048	0.00055
1.4	10.0	0.074	0.00012

the single ions and the pairs. As a result, Birgeneau estimated an accuracy of an order of magnitude in his result. Nevertheless, the values shown in Table II are more than two orders of magnitude smaller. It may be that Model 1 includes too many closely spaced pairs (<10 Å) forcing an underestimate of J_0 in attempting to fit the experimental results.

With macroscopic broadening, since $\delta=0$ for all pairs and $P(\delta=0)=1$, only those energy transfers accompanied by a change in the ground-state energy produce a phonon shift out of the resonance so that

$$W_{\rm ph}^{\rm res}({\rm tot}) = bT_1^{-1}\int_{R_0}^{\infty}\frac{\rho(r)J^2(r)\,dr}{[2J(r)\pm(0.38\ {\rm cm}^{-1})]^2}\ . \tag{14}$$

Using reasonable values of $J_0(10^2-10^3\ {\rm cm}^{-1})$ leads to values of $W_{\rm ph}^{\rm res}({\rm tot})$ for the ground-state energy shift term which are 2–5% of those observed. $W_{\rm ph}^{\rm res}({\rm tot})$ in Model 1 is extremely insensitive to an increase in J_0 due to the effective cutoff on the maximum value of J for Model 1 such that $J(R_0)\leq 1.5h\Delta\nu_{\rm res}$. Increasing J_0 simply increases the range in r which makes the major contribution to the integral with a small resulting increase in $W_{\rm ph}^{\rm res}({\rm tot})$ due to the factor $\rho(r)\propto r^2$.

For the calculation of Model 2 and microscopic broadening we start with the same exponentially decaying spatial dependence for the exchange $J=J_0e^{-ar}$, but with combinations of a and J_0 which are consistent with the Cr_2O_3 exciton results, $J=10\ {\rm cm}^{-1}$ at 3.5 Å. The lower integration limit in Eq. (10) is now selected so as to fit the 0.081% results. The optical and phonon-resonance linewidths are allowed to vary as in Model 1. The results are shown in Table III. With reasonable values for the concentration dependence of the optical linewidth δE, the concentration dependence of τ^{-1} can now be successfully described. Similar results can be obtained with other parameters for the exchange as shown in Table IV. In Model 2 only pairs outside the range 8–10 Å are active in RPAET. Note also that $J(13\ \text{Å})$ is still about one to two orders of magnitude smaller than estimated by Birgeneau. Because of its ability to correctly describe the concentration dependence of the large N^* value of τ^{-1} and its ability to do so with reasonable values of the exchange at 3.5 Å, we consider Model 2 to be closer to a description of the RPAET contribution to the phonon loss in ruby.

TABLE III. Comparison of calculated and experimental phonon loss rates at large N^* for Model 2 with microscopic broadening.

Cr^{3+} conc. (wt%)	δE (cm^{-1})	$h\Delta\nu_{\rm res}$ (cm^{-1})	τ^{-1} ($10^6\ s^{-1}$) Calc. RPAET	Expt.
0.023	0.15	0.016	0.46	0.5
0.081	0.2	0.019	1.02[a]	1.0
0.28	0.3	0.026	1.76	1.7

[a] R_0 was varied to fit the 0.081% data with $a=1$ Å^{-1}, $J_0=330\ {\rm cm}^{-1}$ yielding $R_0=11.0$ Å.

TABLE IV. Alternate sets of exchange parameters a and J_0 and integration limit R_0 in Eq. (10) which fit the 0.081% data in Model 2.

a (Å^{-1})	J_0 (cm^{-1})	R_0 (Å)	$J(13\ \text{Å})$ ($10^{-3}\ cm^{-1}$)
1.0	330	11.0	0.74
1.2	667	9.6	0.11
1.4	1343	8.6	0.017

With no local energy mismatch ($\delta=0$) in Model 2 the ground-state energy shifting term is adequate to explain the observed τ^{-1} but with a smaller value of $R_0(7-8\ \text{Å})$. However, the RPAET contribution to the phonon loss is strictly proportional to n_0, contrary to experiment. Because of the inability of both Models 1 and 2 to explain the magnitude or n_0 dependence of RPAET in the absence of local-energy mismatch, we favor a picture of ruby which contains at least some microscopic broadening.

Despite the inability of either model to determine the absolute magnitude of the RPAET contribution to the phonon loss without an empirical fit to the data, both models predict an identical N^* dependence which is in good accord with experiment as shown in Fig. 4 for the 0.081% sample. The model (solid curve) correctly predicts the independence of τ^{-1} on N^* and spot size for $N^*\geq 10^{18}\ {\rm cm}^{-3}$. For $N^*\geq 3\times 10^{18}\ {\rm cm}^{-3}$ the models also correctly predict the decrease in τ^{-1} due to the depletion of the ground-state concentration n_0. At $N^*=10^{19}\ {\rm cm}^{-3}$, for instance, 40% of the Cr^{3+} ions are excited. The solid curves in Figs. 5 and 6 are the calculated rates for the 0.023 and the 0.28% samples, respectively, using Model 2 and parameters identical to those of the 0.081% sample except for the linewidth changes described above.

Since RPAET can be seen from Figs. 4–6 to dominate the phonon loss rate only at large N^*, we have subtracted this rate from the total experimental rate in order to display the N^* dependence of the remaining mechanisms. The difference between the experimental rates and the RPAET rates are shown in Fig. 9. The data for all three concentrations are con-

TABLE V. Dependence of the relaxation time on the size of the excited region ($L=2R$) and the density of excited ions (N^*).

Spectral redistribution:	
Gaussian line shape	$\tau^{-1} \propto (N^*L)^{-1}F$
Lorentzian line shape	$\tau^{-1} \propto (N^*L)^{-1/2}$
Spatial diffusion ($b >> 1$):	$\tau^{-1} \propto (N^*L)^{-2}$

sistent with a rate which varies as $(N^*)^{-n}$, where $0.8 \leq n \leq 1.0$. It is now possible to draw some conclusions from the data shown in Fig. 9 for the non-RPAET portion of the phonon loss rate τ^{-1}. In the bottlenecked regime, spatial diffusion and spectral redistribution can lead to phonon escape from the excited volume of the crystal. Giordmaine and Nash[31] treated the case of phonon bottlenecking in detail and calculated the dependence of the bottlenecked relaxation time on the size of the excited region ($L=2R$) and the density of excited ions (N^*) for both Gaussian and Lorentzian line shapes. Their results expressed in terms of the rate are summarized in Table V. F is a very weakly dependent function of N^* and L. The data presented in Fig. 9 have a concentration and size dependence approximately of the form

$$\Delta\tau^{-1} \propto (N^*)^{-1}(L)^{-3/2} ,$$

which are most closely consistent with a Gaussian $\bar{E} \rightarrow 2\bar{A}$ resonance line shape with spectral redistribution mainly responsible for the non-RPAET phonon loss rate over the range of N^* covered in these experiments. A similar conclusion was obtained in some of the cw experiments.[8] Spatial diffusion is not observed since for $b >> 1$, the diffusion times are not rate limiting under the conditions of these experiments.

Anharmonic decay should be most evident at small b since the contribution of the anharmonic decay to τ^{-1} is

$$\tau_{AH}^{-1} = T_{AH}^{-1}(1+b)^{-1} ,$$

where T_{AH} is the intrinsic phonon anharmonic decay time. It should also exhibit an independence on spot size. However, the low b data in 0.023% ruby exhibit a strong dependence on spot size, providing a limit $T_{AH} > 10$ μs. Since anharmonic decay is due predominantly to decay of longitudinal phonons which represent only 10% of the active phonons, a lower limit of ~ 1 μs can be established for the anharmonic lifetime of longitudinal 29-cm^{-1} phonons.

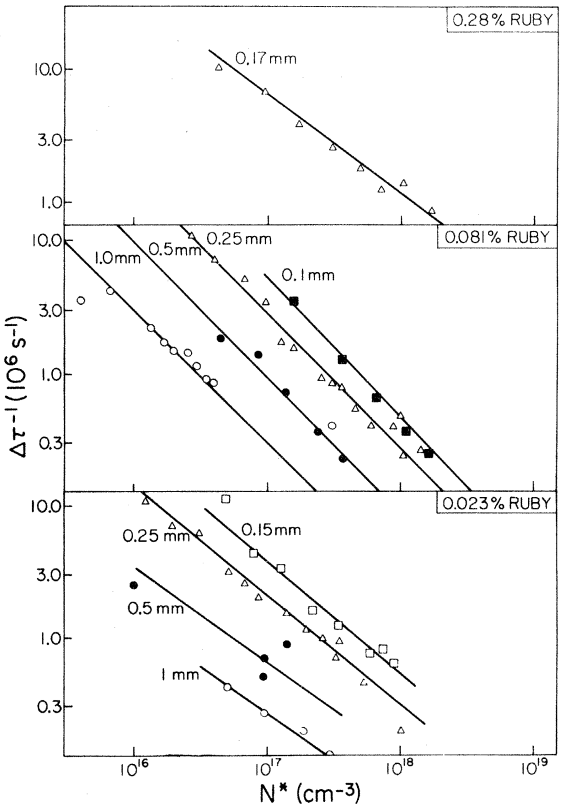

FIG. 9. Non-RPAET contribution to the experimental decay rates as a function of N^* and spot size. These data are obtained by subtracting the RPAET rates shown in Figs. 4–6 from the experimental rates.

V. CONNECTION WITH ENERGY TRANSFER EXPERIMENTS IN RUBY

The RPAET process which limits τ^{-1}, the effective R_2 lifetime in these pulsed laser experiments, is identical to the process which had been predicted to dominate the nonresonant energy transfer in ruby.[18] It is therefore of great interest to compare the results of the phonon experiments with those of energy-transfer experiments in ruby such as fluorescence line narrowing (FLN) and transient grating experiments.

Based on the linear dependence on temperature of the transfer rate and the simultaneous appearance of the full inhomogeneous background, it was concluded in the FLN experiments of Selzer *et al.*[20] that the single-phonon process dominated the nonresonant energy transfer in 1% ruby below 50 K. This was quite surprising in view of the results of Holstein, Lyo, and Orbach[18] who showed that (1) the single-phonon process should make only a small contribution and (2) that of the possible two-phonon processes, the resonant processes (RPAET) should dominate in the 5–50-K temperature range in 1% ruby. Computer simulations of RPAET were per-

formed by Holstein, Lyo, and Orbach[32] for 1% ruby in the case of a Gaussian inhomogeneously broadened profile in the nonstochastic approximation. Using Birgeneau's[29] conclusion as to the exchange matrix element for the 13-Å average separation of nearest neighbor in 1% ruby of $J=2.5\times10^{-3}$ cm^{-1}, they estimated a transfer time of 0.3 ms at 10 K and 15 μs at 40 K, about two orders of magnitude shorter than observed by Selzer *et al.*[20] In addition, the RPAET transfer rate was expected to show an exponential dependence on temperature, contrary to experiment. Suppose, however, that we reduce the value of the exchange at 13 Å by one order of magnitude, based on the results of Sec. V. This reduces the effect of RPAET in the FLN experiments by up to two orders of magnitude ($\propto J^2$), leading to transfer times of 10 and 1 ms at 4.2 and 50 K, respectively. Thus below 50 K observation of RPAET in the FLN experiments in 1% ruby begins to become marginal.[33] A stochastic treatment of the energy transfer, including the possibility of weak links in the energy-transfer chain would certainly further limit the role of RPAET in both FLN and transient grating experiments.

We next examine the transient grating experiments[21] which set an upper limit of 300 Å on the energy transport in the $2\bar{E}$ state of $\sim1\%$ ruby from 10 K to room temperature. These experiments measure the contribution from both resonant and nonresonant energy transfer. We first examine the nonresonant (RPAET) contribution to the transfer. Using Birgeneau's estimate of $J=2.5\times10^{-3}$ cm^{-1} for the 13-Å mean Cr^{3+} separation, we find a typical transfer rate for a $\delta=0.25$ cm^{-1} energy mismatch of

$$(J^2/\delta^2)\,T_1^{-1}e^{-42/T}\simeq10^5e^{-42/T}\ .$$

Diffusion of 300 Å would require times of 400 and 4 ms at 10 and 100 K, respectively. Thus one might expect a measurable contribution at higher temperatures. However, if J at 13 Å is reduced by even one order of magnitude, 300-Å diffusion times for RPAET become larger than 400 ms even at the highest temperatures.

Turning to the resonant contribution we note that in the approximation of microscopic strain broadening, the exchange contribution to the resonant part of the spatial energy transfer is negligible. Assuming a ratio of homogeneous to inhomogeneous widths of 10^{-2}, nearest-neighbor Cr^{3+} ions are separated on the average by ~40 Å in 1% ruby. At these distances multipolar transfer will certainly dominate the short-range exchange. In fact, experiments with a Stark field pseudosplitting indicate very slow resonant transfer.[22]

Finally we ask why RPAET plays a dominant role in the resonant-phonon dynamics, but is not seen in energy-transfer experiments. It is the relatively small number of strongly coupled pairs ($r\simeq10$–12 Å), whose excitation energy is transferred back and forth between the members of the pair by the resonant phonons which act repeatedly, thus shifting the phonons out of the resonance. The excitation energy remains localized within the group of strongly coupled ions for a long time before transfer across a weak link in the interaction can occur. Therefore long-range energy transport occurs slowly despite the rapid energy transfer between the two members of the strongly coupled pairs. Only $\simeq5\%$ of the Cr^{3+} ions are involved in the pairs which make a significant contribution to RPAET. The bulk of the ions, which are the ones sampled in a FLN experiment, remain too weakly coupled with the reduced values of J required for interpretation of the RPAET experiments to transfer their energy within the Cr^{3+} radiative lifetime, even at 50 K.

VI. CONCLUSIONS

Although our understanding of the dynamics of resonantly trapped 29-cm^{-1} phonons in ruby is not complete, we can draw several conclusions about both the phonons and energy transfer. (1) For Cr^{3+} concentrations in excess of $c=0.03$ wt%, resonant-phonon-assisted energy transfer (RPAET) dominates the phonon loss in the high N^* region ($N^*c\gtrsim10^{17}$ wt% cm^{-3}). (2) Comparison of calculations on the magnitude of RPAET with experiment leads us to conclude that previous estimates of the exchange contribution to energy transfer in the ^2E states of ruby may be too large by about one order of magnitude, at least at mean pair distances in 1% ruby ($r\simeq13$ Å), and that this explains why RPAET was not seen in the fluorescence line-narrowing experiments. (3) We find that for the models considered in this work, only the assumption of some microscopic broadening can successfully describe all of the observations including the magnitude and concentration dependence of RPAET. (4) A mechanism exists, in addition to pure spatial diffusion, which contributes to the resonant-phonon loss at moderate values of N^* which seems to be most consistent with the model of spectral diffusion of Giordmaine and Nash[30] for a Gaussian-shaped resonance. (5) No evidence for anharmonic decay of 29-cm^{-1} phonon is observed in our experiments and we conclude that the anharmonic decay time of 29-cm^{-1} longitudinal phonons is $\gtrsim1$ μs.

Finally, we emphasize that there remain large differences in the results of the pulsed and cw experiments and within the cw experiments themselves which, at this point, are totally unexplained. Problems remain, therefore, both experimentally and theoretically, in our understanding of the dynamics of resonantly trapped 29-cm^{-1} phonons in ruby.

ACKNOWLEDGMENTS

We express our gratitude to Ray Orbach and S. K. Lyo for their comments on several occasions, and to L. A. Godfrey for his assistance in the development of the flashlamp-pumped dye laser system. We are grateful for support from the U.S. Army Research Office, Durham, under Grant No. DAAG 29-78-G-0107.

---

*Present address: 3M Central Research Laboratory, P. O. Box 33221, St. Paul, Minn. 55133.

[1]S. Geschwind, G. E. Devlin, R. L. Cohen, and S. R. Chinn, Phys. Rev. 137, A1087 (1965).

[2]R. Adde, S. Geschwind, and L. R. Walker, in *Proceedings of the Fifteenth Colloque Ampere,* edited by P. Averbuch (North-Holland, Amsterdam, 1969), p. 460.

[3]K. F. Renk, in *Proceedings of the Second International Conference on Light Scattering in Solids,* edited by M. Balkanski (Flammarion, Paris, 1971), p. 12.

[4]K. F. Renk and J. Peckenzell, J. Phys. (Paris) 33, C4-103 (1972).

[5]A. A. Kaplyanskii, S. A. Basun, V. A. Rachin, and R. A. Titov, Pis'ma Zh. Eksp. Teor. Fiz. 21, 438 (1975) [JETP Lett. 21, 200 (1975)].

[6]S. A. Basun, A. A. Kaplyanskii, V. A. Rachin and R. A. Titov, Akust. Zh. 22, 599 (1976) [Sov. Phys. Acoust. 22, 333 (1976)].

[7]A. A. Kaplyanskii, S. A. Basun, V. A. Rachin and R. A. Titov, Fiz. Tverd. Tela (Leningrad) 17, 3661 (1975) [Sov. Phys. Solid State 17, 2380 (1976)].

[8]J. I. Dijkhuis, A. van der Pol, and H. W. de Wijn, Phys. Rev. Lett. 37, 1554 (1976).

[9]R. S. Meltzer and J. E. Rives, Phys. Rev. Lett. 38, 421 (1977); in *Proceedings of the International Conference on Lattice Dynamics,* edited by M. Balkanski (Flammarion, Paris, 1978), p. 777.

[10]G. Pauli and K. F. Renk, in *Proceedings of the International Conference on Lattice Dynamics,* edited by M. Balkanski (Flammarion, Paris, 1978), p. 232.

[11]G. Pauli, K. F. Renk, G. Klimke, and H. J. Kreuzer, Phys. Status Solidi 95, 503 (1979).

[12]G. Pauli and K. F. Renk, Phys. Lett. A 67, 410 (1978).

[13]J. I. Dijkhuis and H. W. de Wijn, Phys. Rev. B 20, 1844 (1979).

[14]W. C. Egbert, R. S. Meltzer, and J. E. Rives, in *Phonon Scattering in Condensed Matter,* edited by H. J. Maris (Plenum, New York, 1980), p. 365.

[15]A. A. Kaplyanskii, S. A. Basoon, and V. L. Shekhtman, in *Light Scattering in Solids,* edited by J. L. Birman, H. Z. Cummins, and K. K. Rebane (Plenum, New York, 1979), p. 95.

[16]I. B. Levinson, Zh. Eksp. Teor. Fiz. 75, 234 (1978) [JETP 48, 117 (1978)].

[17]V. A. Malyshev and V. L. Shekhtman, Opt. Spektrosk. 46, 800 (1979) [Opt. Spectrosc. (USSR) 46, 446 (1979)].

[18]T. Holstein, S. K. Lyo, and R. Orbach, Phys. Rev. Lett. 36, 891 (1976).

[19]P. Hu, Phys. Rev. Lett. 44, 417 (1979).

[20]See, for instance: P. M. Selzer, D. L. Huber, B. B. Barnett and W. M. Yen, Phys. Rev. B 17, 4979 (1978).

[21]P. F. Liao, L. M. Humphrey, D. M. Bloom, and S. Geschwind, Phys. Rev. B 20, 4145 (1979).

[22]P. E. Jessop and A. Szabo, Phys. Rev. Lett. 45, 1712 (1980); S. Chu, H. M. Gibbs, and S. L. McCall, and A. Passner, *ibid.* 45, 1715 (1980).

[23]D. M. Dood, D. L. Wood, and R. L. Barns, J. Appl. Phys. 35, 1183 (1964).

[24]R. S. Meltzer and R. M. Wood, Appl. Opt. 16, 1432 (1977).

[25]R. S. Meltzer and J. E. Rives, Phys. Rev. B 15, 2442 (1977).

[26]T. Holstein, S. K. Lyo, and R. Orbach, in *Topics in Applied Physics,* edited by W. M. Yen and P. M. Selzer (Springer-Verlag, Heidelberg, New York, 1981), Vol. 49, Chap. 2.

[27]S. K. Lyo, Phys. Rev. B 3, 3331 (1971).

[28]J. W. Allen, R. M. Macfarlane, and R. L. White, Phys. Rev. 179, 523 (1969).

[29]R. J. Birgeneau, J. Chem. Phys. 50, 4282 (1969).

[30]G. F. Imbusch, Phys. Rev. 153, 326 (1967).

[31]J. A. Giordmaine and F. R. Nash, Phys. Rev. 138, A1510 (1965).

[32]T. Holstein, S. K. Lyo, and R. Orbach, Phys. Rev. B 15, 4693 (1977).

[33]We duly note, however, that a reduction of the exchange at 13 Å presents an additional problem in understanding how the single-phonon process can mediate nonresonant energy transfer since its probability is also proportional to J^2 as described in Ref. 26.